High-Temperature Processing of $Ba_3ZnTa_2O_9$: an In situ Study Using Synchrotron X-ray Powder Diffraction

Phillip M. Mallinson,[†] John B. Claridge,[†] Matthew J. Rosseinsky,*[,†] Richard M. Ibberson,*[,‡] Jonathan P. Wright,[§] and Andrew N. Fitch[§]

Department of Chemistry, The University of Liverpool, Liverpool L69 7ZD, United Kingdom, ISIS Facility, STFC−Rutherford Appleton Laboratory, Harwell Science and Innovation Campus, Didcot, Oxon OX11 0QX, United Kingdom, and European Synchrotron Radiation Facility, BP-220, F-38043 Grenoble Cedex 9, France

Received May 9, 2007. Revised Manuscript Received July 2, 2007

In situ synchrotron X-ray powder diffraction is used to study the kinetics of cation ordering and ordered domain growth in the microwave dielectric electroceramic $Ba_3ZnTa_2O_9$ (BZT) with a time resolution of 15 s and processing temperatures of up to 1500 °C. This permits the measurement of the activation energy for cation ordering and the identification of different mechanisms for ordered domain growth, associated with the formation of the $Ba_8ZnTa_6O_{24}$ impurity phase due to zinc loss.

Introduction

Production and processing of commercial dielectric resonators for use in mobile telecommunication base stations requires optimization of three figures of merit. These are a high relative permittivity ($\epsilon_r \approx 30$), a low dielectric loss at microwave frequencies ($Q = 1/\tan\delta \approx 50\,000-70\,000$) and a minimal temperature coefficient of the resonance frequency ($\tau_f \approx 0$). One such family of dielectric resonators that has the required properties is based on the B-site ordered perovskite $Ba_3ZnTa_2O_9$ (BZT);[1,2] however, production of these materials is not straightforward and requires a carefully controlled two-stage high-temperature synthesis. The initial synthesis of BZT (calcination stage) from the appropriate oxide and carbonate precursors results in a material that has poor resonator properties due to high loss (low *Q*), attributed to site occupancy disorder of the Zn and Ta cations on the octahedral B-site of the cubic perovskite structure.[3,4] Crucially, a second high-temperature processing step is required to induce the required 2:1 B-site cation ordering in BZT.[5] This ordering consists of single layers of ZnO_6 octahedra alternating with bilayers of TaO_6 along the crystallographic *c*-axis of the trigonal cell (one of the <111> directions of the perovskite cell). The enhanced cation ordering is quantified by the spatial extent of the ordered domains and the magnitude of the order parameter (*OP*), where *OP* is defined as the extent of Zn and Ta segregation over the two octahedral sites. The ordering and hence the Q value for BZT has been found to be very sensitive to the processing conditions.[1] Further complications during processing arise because of the loss of zinc from the material at high temperatures, leading to Zn-deficient impurity phases,[6,7] and the possible existence of some short-range 1:1 ordering, especially with lower processing temperatures.[8] Similar complex issues affecting cation ordering and processing have also been reported recently in the related $Ba_3ZnNb_2O_9$ (BZN) system.[9]

Detailed study of the in situ processing of BZT is a difficult task because of the high temperatures required for the ordering step, typically 1200−1500 °C. Ex situ characterization has revealed details of ordering and Zn loss while also highlighting the extreme sensitivity to processing and the ultimately biphasic nature of annealed BZT; the phase-separation is between essentially fully ordered and partially ordered and likely Zn-deficient phases.[10] In situ studies are especially attractive in that they allow the observation of the evolution of key structural parameters in real time and may also show transient effects that are not observed in an ex situ study. In our previous work,[11] the annealing of BZT at 1200 °C was studied by in situ synchrotron X-ray powder diffraction. In that study, the maximum temperature was limited to some 1200 °C, the upper limit for reliable use of the furnace at that time; however, at this temperature the rate of the cation ordering during processing was also appropriately matched to the comparatively long (ca. 2 h)

* To whom correspondence should be addressed. E-mail: m.j.rosseinsky@liverpool.ac.uk (M.J.R.); r.m.ibberson@rl.ac.uk (R.M.I.).
[†] The University of Liverpool.
[‡] STFC−Rutherford Appleton Laboratory.
[§] European Synchrotron Radiation Facility.

(1) Desu, S. B.; O'Bryan, H. M. *J. Am. Ceram. Soc.* **1985**, *68*, 546−551.
(2) Tamura, H.; Konoike, T.; Sakabe, Y.; Wakino, K. *J. Am. Ceram. Soc.* **1984**, *67*, C59−C61.
(3) Kawashima, S.; Nishida, M.; Ueda, I.; Ouchi, H., *J. Am. Chem. Soc.* **1983**, *66*, 421−423.
(4) Sagala, D. A.; Nambu, S. *J. Am. Ceram. Soc.* **1992**, *75*, 2573−2575.
(5) Jacobson, A. J.; Collins, B. M.; Fender, B. E. F. *Acta Crystallogr., Sect. B* **1976**, *32*, 1083−1087.
(6) Moussa, S. M.; Claridge, J. B.; Rosseinsky, M. J.; Clarke, S.; Ibberson, R. M.; Price, T.; Iddles, D. M.; Sinclair, D. C. *Appl. Phys. Lett.* **2003**, *82*, 4537−4539.
(7) Thirumal, M.; Davies, P. K. *J. Am. Ceram. Soc.* **2005**, *88*, 2126−2128.
(8) Barber, D. J.; Moulding, K. M.; Zhou, J.; Li, M. Q. *J. Mater. Sci.* **1997**, *32*, 1531−1544.
(9) Wu, H.; Davies, P. K. *J. Am. Ceram. Soc.* **2006**, *89*, 2239−2249.
(10) Bieringer, M.; Moussa, S. M.; Noailles, L. D.; Burrows, A.; Kiely, C. J.; Rosseinsky, M. J.; Ibberson, R. M., *Chem. Mater.* **2003**, *15*, 586−597.
(11) Moussa, S. M.; Ibberson, R. M.; Bieringer, M.; Fitch, A. N.; Rosseinsky, M. J. *Chem. Mater.* **2003**, *15*, 2527−2533.

10.1021/cm071249j CCC: $37.00
Published on Web 08/23/2007

data collection time required for the measurements with high angular resolution. In this paper, high-intensity lower-resolution synchrotron X-ray powder diffraction is used, combined with a superior furnace performance, to enable the processing of BZT to be investigated in situ with a much-improved time resolution of 15 s and up to commercially important processing temperatures of 1500 °C.

Experimental Section

Polycrystalline samples of $Ba_3ZnTa_2O_9$ were synthesized using stoichiometric amounts of $BaCO_3$ (Solvay), ZnO (Durham Electrox 2500), and Ta_2O_5 (H. C. Starck). The starting materials were placed in a 25 cm^3 polypropylene bottle half-filled with magnesia-stabilized zirconia milling media, 10 mL of distilled water was added before milling for 16 h. The dried powders were calcined at 1000 °C for 2 h. The calcined powders were loaded into Pt capillaries with internal diameter 0.52 mm and wall thickness 0.04 mm. Powder X-ray diffraction data were collected on the ID11 beamline at the European Synchrotron Radiation Facility (ESRF), Grenoble, France. A wavelength of 0.3473 Å was selected as a compromise between the need for hard X-rays in order to minimize absorption by Pt while avoiding the Ba K edge at 0.3311 Å. A Bruker Smart 65000 area detector was used with a 5 s data collection and 10 s readout period, giving a data set every 15 s.

High-temperature measurements were made using an optical furnace comprising three 150 W halogen bulbs mounted on a ceramic body. The bulbs focus onto a 4 mm section along the sample capillary axis; therefore, conventional measurement of the sample temperature using a thermocouple during data collection is impossible. Power settings for the furnace were calibrated initially off-line using a thermocouple in place of the capillary. Temperature measurement during the in situ experiments was achieved by monitoring the unit-cell volume of the Pt capillary and comparing this with thermal expansion values determined from in situ neutron powder diffraction experiments[12] using a type W5 thermocouple. The temperature stability of the furnace was typically ±25 °C.

At the start of the experiment, the power to the furnace was stepped up to the reaction temperature over a period of approximately 20 min to maximize the lifetime of the halogen bulbs. The experiment was considered to start ($t = 0$) when this temperature was reached. In every case, no superlattice intensity consistent with cation order was observed at $t = 0$, although the subcell reflections were already sharper compared to the calcined starting material. Four separate experiments were performed: (a) annealing at 1200 °C for 18 000 s and then ramping to 1450 °C for 2400 s, (b) annealing at 1300 °C for 14 400 s, (c) annealing at 1400 °C for 3600 s, and (d) annealing at 1500 °C for 4500 s.

Results

After the initial calcination step, the crystal structure of the product, determined by laboratory powder X-ray diffraction, was that of a B-site disordered cubic perovskite, as shown in Figure 1. Ordering of the Ta and Zn cations on the B-sites leads to a trigonal distortion of the cubic perovskite unit cell, see Figure 1, and the appearance of superstructure peaks in the X-ray diffraction pattern, the strongest of these being the (001) and (100) reflections of the trigonal cell. The intensity of these superstructure reflections is approximately proportional to the extent of

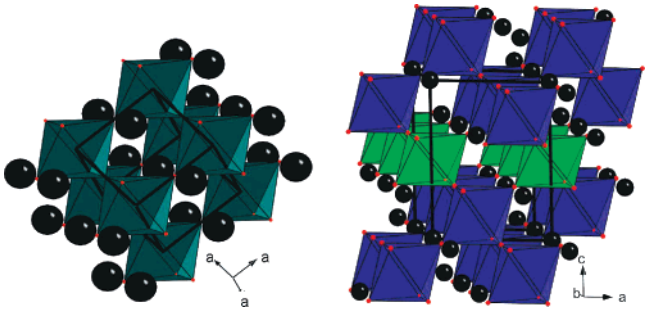

Figure 1. Illustration of the crystal structure of the disordered cubic perovskite subcell (left, <111> direction vertical) and the ordered trigonal supercell ($P\bar{3}m1$) (right, *c*-axis vertical) of $Ba_3ZnTa_2O_9$ showing layers of TaO_6 (blue) and ZnO_6 (green) octahedra.

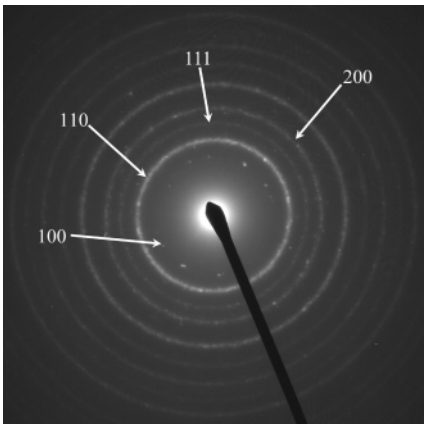

Figure 2. Electron diffraction image of the calcined $Ba_3ZnTa_2O_9$ starting material. Miller indices are for the cubic B-site disordered subcell; no superstructure reflections indicative of cation ordering are observed.

ordering (when ignoring incomplete site occupation and Debye−Waller factor effects). The superstructure reflections associated with the ordering were not observed in the calcined starting material. Investigation of the starting material by electron diffraction showed the particle size to be smaller than the probe size, and this resulted in the observed powder rings seen in Figure 2. Indexing the pattern on the disordered cubic cell gives $a = 4.1$ Å. The (100) reflection of the cubic cell can only be observed as a series of dots. The (100) reflection is quite weak compared to the other reflections observed, consistent with only a limited number of particles being in the correct orientation. The superstructure reflections indicative of ordering were not observed in the five separate electron diffraction studies made.

Each 15 s synchrotron data set was analyzed sequentially using the Rietveld method implemented in the GSAS suite of programs.[13] The ID11 powder diffraction data are of lower resolution compared with previous studies;[10−12] therefore, a structural model using a single trigonal phase of BZT was adequate to fit the data. For each experiment, atomic coordinates and isotropic displacement parameters, which were constrained to be equal for each atom type, were refined against the final data set recorded at the end of the annealing period. These values were then used as fixed parameters in the subsequent analysis (final atomic coordinates for the

(12) Ibberson, R. M.; Moussa, S. M.; Rosseinsky, M. J.; Fitch, A. N.; Iddles, D.; Price, T., *J. Am. Ceram. Soc.* **2006**, *89*, 1827−1833.

(13) Larson, A. C.; Dreele, R. B. V. *General Structure Analysis System (GSAS)*, Los Alamos National Laboratory Report LAUR 86-748; Los Alamos National Laboratory: Los Alamos, NM, 2004.

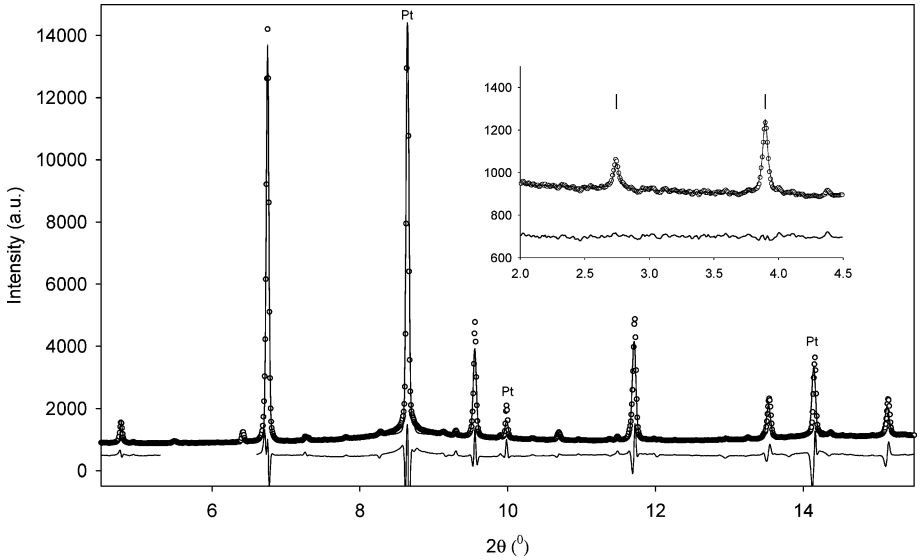

Figure 3. Result of the profile fitting for the data set recorded at 1300 °C after 10 000 s annealing. The main figure corresponds to histogram 1 containing BZT subcell reflections and Pt with R_{wp}=9.10%, R_p=5.23%, and χ^2=10.39. Inset is shown the (001) and (100) BZT supercell reflections fitted as a second histogram with separate lattice constants (see text) with R_{wp} = 1.50%, R_p 0.89%, and χ^2 = 0.21.

1300 °C experiment are given in Table S1 of the Supporting Information). Structural variables in the sequential refinement procedure comprised the cation site occupancies, constrained to maintain correct stoichiometry, and unit cell parameters. The observed reflections from the Pt capillary indicated a strong texture of the material, which evolved during the high-temperature measurements, and were therefore best modeled using the Le Bail method to fit the individual peak intensities. The volatility of Zn results in impurity phases forming, most notably $Ba_8ZnTa_6O_{24}$[6,7] at higher annealing temperatures. At the highest temperatures studied (1450 and 1500 °C), a substantial amount of $Ba_8ZnTa_6O_{24}$ formed and this phase was included in the refinement model, accounting for 7 and 9 wt % of the sample at the end of the respective annealing periods.

The peak shape of the BZT reflections was fitted using the Lorentzian (LX term) in the GSAS type 2 peak shape function. The diffraction data were of sufficient resolution to discriminate between broad supercell reflections and the sharper subcell reflections; this was managed in the profile refinement procedure by splitting these two families of reflections into separate histograms. The first histogram included solely the subcell BZT reflections and all Pt reflections; the second covered only the BZT supercell reflections. Accordingly, an indication of the ordered domain size, p (Å), can be calculated from the fwhm of the supercell peaks, converted to integral breadths,[13,14] using the formula

$$p = 36000K\lambda/\pi^2X \qquad (1)$$

where K is the Scherrer constant (assumed to be 1.0 corresponding to spherical crystallites), λ is the incident wavelength in Å, and X is the peak width parameter LX refined for the supercell peaks. The instrumental contribution to the peak shape was parametrized by fitting data recorded using a sample of LaB_6 (NIST standard reference material 660a) under the same experimental setup and gave a negligible contribution to the Lorentzian size-broadening parameter. The refined scale factors for each histogram were constrained to be equal and the background was fitted to each histogram using separate tenth-order and sixth-order polynomial functions, respectively.

Refinement of the Ta/Zn occupation over the B-sites in the trigonal structure was constrained to stoichiometric values allowing the calculation of the order parameter (*OP*) defined as

$$OP(\mathrm{Ta}) = (n\mathrm{Ta}(2d) - n\mathrm{Ta}(1b))/(n\mathrm{Ta}(2d) + n\mathrm{Ta}(1b)) \qquad (2)$$

where 2*d* and 1*b* denote the Wyckoff positions in the $P\bar{3}m1$ space group. In an ideal case, when $OP = 0$, the material is fully disordered, and when $OP = 1$, the material is fully ordered. However, on a microscopic level, the role of antiphase domain boundaries, where there is a fault in the 2:1 stacking sequence, complicates this picture. Any increase in *OP* must at least be partially attributed to the increasing domain size during annealing, lowering the concentration of the domain boundaries. Typical results of the Rietveld fitting are shown in Figure 3.

Discussion

Cation Ordering. The kinetics of solid-state transformations can be analyzed according to the theory of nucleation and growth processes developed independently by Kolmogorov,[15] Johnson and Mehl,[16] and Avrami.[17−19] The KJMA theory for a homogeneous reaction, requires that the probability of any small region transforming in a given period of time is the same throughout the volume of material. Thus,

(14) Balzar, D.; Audebrand, N.; Daymond, M. R.; Fitch, A.; Hewat, A.; Langford, J. I.; Le Bail, A.; Louer, D.; Masson, O.; McCowan, C. N.; Popa, N. C.; Stephens, P. W.; Toby, B. H. *J. Appl. Crystallogr.* **2004**, *37*, 911−924.

(15) Kolmogorov, A. N. *Bull. Acad. Sci. USSR Ser. Math.* **1939**, *3*, 355−359.
(16) Johnson, W. W.; Mehl, R. F. *Trans. AIME* **1939**, *135*, 416−422.
(17) Avrami, M. *J. Chem. Phys.* **1940**, *7*, 1103−1112.
(18) Avrami, M. *J. Chem. Phys.* **1940**, *8*, 212−224.
(19) Avrami, M. *J. Chem. Phys.* **1941**, *9*, 177−184.

the volume transforming in a short time period is proportional to the remaining untransformed volume at the beginning of the interval. The transformed volume, V^{β}, follows a first-order relation to the total volume, V, according to

$$dV^{\beta}/dt = k(V - V^{\beta}) \quad (3)$$

and by integrating

$$V^{\beta}/V = 1 - \exp(-kt) \quad (4)$$

Where t is time, k is the rate constant, and V^{β}/V is equivalent to the order parameter. The mechanism of particle growth, e.g., instantaneous or continuous nucleation, growth in less than three dimensions, and heterogeneous nucleation, is reflected by the Avrami exponent, n, of t,[20] to give

$$V^{\beta}/V = 1 - \exp(-kt^{n}) \quad (5)$$

For $n = 1$, the transformation curve is equivalent to that of a first-order homogeneous reaction and for other values of n, the curves of V^{β}/V take a sigmoidal form, the fractional volume initially increases slowly, then more rapidly before slowing again. The Avrami exponent, n, is a complex term involving contributions from the nucleation rate (that can be constant, increasing or decreasing) and the dimensionality of the process. In the case where all nucleation sites are saturated at the start of the reaction, the exponent is dependent on the spatial dimensionality, d, of the interface on which growth occurs according to $n = 3 - d$.[20] Grain boundary nucleation and growth implies $d = 2$ and therefore $n = 1$. The present results for ordering of BZT above 1300 °C show $n \approx 1$; hence, nucleation is not considered to be a major factor. The ordering is generally time-dependent and controlled by either domain boundary motion or bulk diffusion. In this case, as no compositional change is involved, domain boundary motion is considered to be the more important effect.

The evolution of the cation order parameter, *OP*, at each of the temperatures studied is shown in Figure 4. The *OP* typically increases rapidly on reaching the annealing temperature and during the initial stages of annealing before saturating at a maximum; this process taking as little as 800 s at 1500 °C. The variation of OP as a function of annealing time was fitted using a modified version of the KJMA model as follows

$$OP(t) = OP_0 + (OP_{\infty} - OP_0)(1 - \exp(-kt)^{n}) \quad (6)$$

In this equation, OP_0 is the order parameter at $t = 0$ (i.e., when the furnace reached the reaction temperature). Inclusion of the OP_0 term was necessary to fit the data and in this case represents the level of ordering in the starting material, although this is not directly observed in the powder diffraction data because the supercell reflections are too broad and/or weak to be observed at $t = 0$. An alternative approach when modeling reaction kinetics is to introduce a time offset, t_0, to account for the induction period required to reach the reaction temperature. This approach yields values of many hours, which is unreasonable given the known induction periods for these experiments, which at most corresponds to 20 min. OP_{∞} is the order parameter at $t = \infty$ and corresponds to the maximum degree of ordering achievable in each experiment.

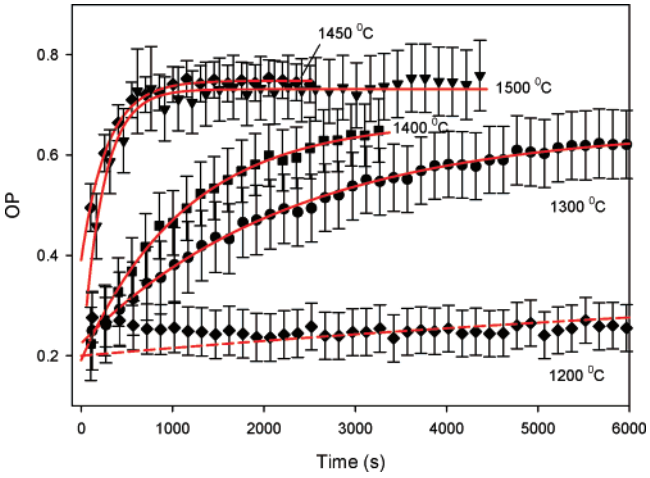

Figure 4. Variation of the cation order parameter (OP) with time at each annealing temperature. Solid lines denote the KJMA model fitting at each temperature with the Avrami exponent, n, fixed at 1.0. The dotted line denotes the predicted OP variation at 1200 °C based on previous results,[11] see text (note: for reasons of clarity, only every 10th data point is shown and data recorded at 1200 and 1300 °C beyond 6000 s are not shown).

At each temperature, excluding the 1200 °C data, the Avrami exponent was treated as a variable parameter in the first instance; however, the refined values did not deviate significantly from 1.0 (1.27(65) at 1300 °C, 1.04(13) at 1400 °C, 1.38(22) at 1450 °C, 1.01(7) at 1500 °C), and hence final analysis was carried out with the exponent fixed at 1.0. The fitted parameters for each experiment are shown in Table 1. At 1200 °C, ordering was not observed within error over the limited time period of the experiment (18 000 s) and no kinetic information could be extracted from these data. However the evolution of cation order in BZT at 1200 °C has been shown previously to follow the same pattern observed at the higher temperatures, albeit over a considerably longer time (up to 50 000 s for maximum ordering).[11] Using the rate constant determined previously at 1200 °C and assuming typical OP_0 and OP_{∞} values of 0.2 and 0.7, respectively (see Table 1), the present observations at 1200 °C are entirely consistent with the predicted behavior on the basis of the earlier measurements.

In the antisite disorder model described above, the ordering is quantified by the OP using the ratio of Zn^{2+}/Ta^{5+} on the 1*b* and 2*d* sites. Increased ordering involves more Ta^{5+} and less Zn^{2+} on the 2*d* site and vice-versa for the 1*b* site. However, this model is problematic when considering switching a Ta^{5+} or Zn^{2+} cation to or from the smaller 2*d* sites or larger 1*b* sites without concomitant changes in the coordination of the oxygen around the site. This apparent chemical discrepancy is supported by the calculation of bond valence sums, which show Ta^{5+} underbonded when on the 1*b* site and Zn^{2+} overbonded when on the 2*d* site. The antisite model, however, remains a good approximation when analyzing the diffraction data not in terms of the local chemical environment of an individual site but rather the average over a very large number of sites. With this

(20) Christian, J. W. *The Theory of Transformations in Metals and Alloys*; Pergamon Press: Oxford, U.K., 1975.

Table 1. Fitted Parameters for the Cation Ordering Using the Antisite Model (upper line) and Stacking-Fault Model (lower line) at Each Temperature According to the Modified KJMA Model: $OP(t) = OP_0 + (OP_\infty - OP_0)(1 - \exp(-kt)^n)$

	1300 °C	1400 °C	1450 °C[a]	1500 °C
k (s^{-1})	4.336(23) × 10^{-4}	8.749(11) × 10^{-4}	3.520(57) × 10^{-3}	4.363(119) × 10^{-3}
	5.715(79) × 10^{-4}	1.243(18) × 10^{-3}	3.495(73) × 10^{-3}	4.126(68) × 10^{-3}
OP_0	0.2246(13)	0.1911(20)	0.3906(35)	0.1717(128)
	0.6925(10)	0.6462(16)	0.7406(16)	0.6721(22)
OP_∞	0.6546(4)	0.6698(20)	0.7482(8)	0.7312(10)
	0.9080(9)	0.9009(9)	0.8712(4)	0.8783(3)

[a] The data at 1450 °C are recorded after preliminary heating to 1200 °C for 18000 s.

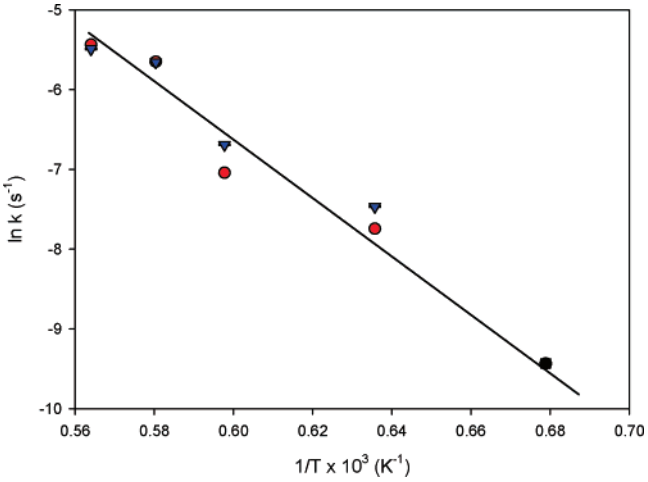

Figure 5. Arrhenius fit to rate constants determined using the antisite order model (circles, present study; square, value taken from[11]). Values determined using the stacking fault model are shown as triangles.

assumption, it is reasonable to exchange Zn^{2+} for Ta^{5+} and to change the local coordination of the sites via oxide anion displacements taken up in the displacement parameters without the refinement being sensitive to the local change in individual bond lengths.

An alternative model for the cation ordering based on translational stacking faults was also used to analyze the data, as suggested by Ting et al.[21] In this case, the disorder is described by the presence of microstructure comprising translational stacking faults. This is characterized by a displacement shift vector across stacking faults of $\pm\mathbf{R}$, where $\mathbf{R} \approx \mathbf{c}_p \equiv 1/3[-\mathbf{a}_h + \mathbf{b}_h + \mathbf{c}_h]$ (subscripts p and h denote perovskite pseudocubic and hexagonal axes, respectively) and when modeled in a Rietveld refinement, the displacement shift is seen as B-site disorder. To refine this model, we require three translational variants of the superstructures. Within each variant, Zn^{2+} resides solely on the 1*b* site and Ta^{5+} solely on the 2*d* site and therefore the local structure can be modeled without under- and overbonding of the cations as seen in the antisite model. The dominant variant *a* is translated to the minor variants *b* and *c* by $-\mathbf{R}$ and $+\mathbf{R}$ (where $\mathbf{R} = [-1/3, 1/3, 1/3 + \delta]$). The degree of order is then quantified by the relative amounts of the variants; a fully ordered material would have exclusively the *a* variant and none of the *b* or *c* variants.

The diffraction data for each experiment were refined using this stacking-fault model in the same way as for the antisite model. The amount of the dominant translational variant (i.e., the measure of the ordering) was extracted for each data set. The curves were fitted to the same KJMA model as used previously for the antisite model; the fitted parameters are in Table 1. Comparing the rates of ordering between the two models shows them to be in good agreement. Because of the way they are quantified, the values of the initial and final ordering cannot be directly compared between the antisite disorder and stacking fault models (final atomic coordinates for the 1300 °C experiment using the stacking-fault model are given in Table S2 of the Supporting Information.)

An Arrhenius plot of the ordering rates determined from the four experiments using both structural models is shown in Figure 5. The calculated activation energies are 338(37) and 336(40) kJ mol^{-1} for the antisite model and the stacking fault model, respectively. These values compare well with the activation energies for cation transport seen in other oxide systems, for example, Fe in $GdFeO_3$, $E_a = 397$ kJ mol^{-1} and in $YFeO_3$, $E_a = 414$ kJ mol^{-1},[22] and Zn in $ZnAl_2O_4$, $E_a = 326$ kJ mol^{-1}.[23]

KJMA models have been used to analyze the kinetics in a number of systems that show similarities to the ordering kinetics observed in BZT. The back transformation of $(Mg_x,Fe_{1-x})_2SiO_4$ ($x = 1$, 0.8. and 0.4) from the spinel to the olivine structure was studied in situ at temperatures between 760 and 900 °C by Ming et al.[24] The olivine phase was shown to grow with time at the expense of the spinel phase. Hence, the transformation was considered to be a heterogeneous transformation involving a nucleation and growth mechanism, i.e., comparable to ordering in BZT. The rate of ordering was found to be between 4.8 × 10^{-6} s^{-1} and 2.0 × 10^{-5} s^{-1} with *n* in the range 1.48−1.56. The values of the Avrami exponent for the spinel to olivine transformation indicate that rapid nucleation is followed by grain boundary nucleation and growth, with an exponent similar to that found here for the ordering in BZT.

The kinetics of ordering in the alloys α-CuAl and Ni_3Al studied by differential scanning calorimetry (DSC) also show similarities to BZT. In α-CuAl, with 19, 13, and 6.5 wt % Al, a nonisothermal study of the ordering gave $E_a = 145-178$ kJ mol^{-1} and $n = 1.39$.[25] The DSC thermograms show two distinct exothermic reactions. The first signal, at lower temperature, is partially attributed to the development of short-range order. The second larger signal is indicative of the development of long-range ordering. The conclusions are

(21) Ting, V.; Liu, Y.; Noren, L.; Withers, R. L.; Goossens, D. J.; James, M.; Ferraris, C., *J. Solid State Chem.* **2004**, *177*, 4428−4442.
(22) Buscaglia, V.; Buscaglia, M. T.; Giordano, L.; Martinelli, A.; Viviani, M.; Bottino, C., *Solid State Ionics* **2002**, *146*, 257−271.
(23) Freer, R., *J. Mater. Sci* **1980**, *15*, 803−824.
(24) Ming, L. C.; Kim, Y. H.; Manghnani, M. H.; Ushadevi, S.; Ito, E.; Xie, H. S. *Phys. Chem. Miner.* **1991**, *18*, 171−179.
(25) Varschavsky, A.; Donoso, E. *Metall. Mater. Trans. A* **1983**, *14*, 875−880.

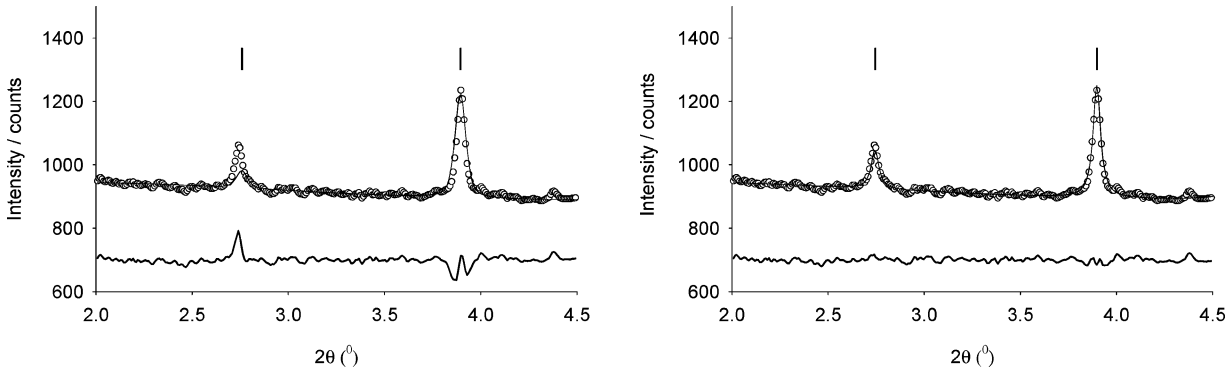

Figure 6. Profile fits to the (001) and (100) supercell peaks for data recorded at 1300 °C at the end of the annealing period. Left, data modeled with common lattice parameters for super- and subcell peaks. Right, data modeled with separate lattice constants for the super- and subcell peaks (as shown in Figure 3).

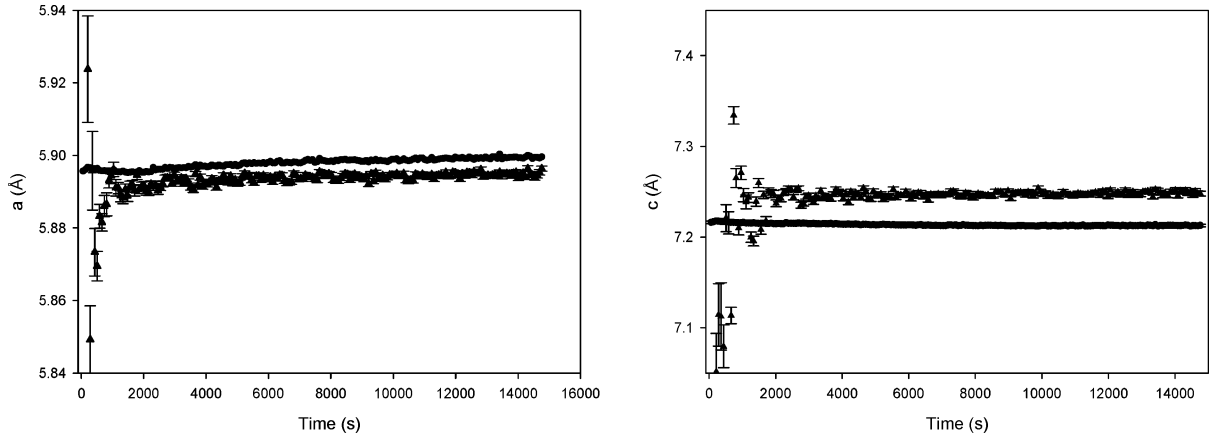

Figure 7. Variation of the *a* (left) and *c* (right) lattice constants at 1300 °C determined from subcell (circles) and supercell (triangles) reflections (note: for reasons of clarity, only every fifth data point is shown). Figure S1 in the Supporting Information shows the variation of lattice constants at 1400 , 1450, and 1500 °C.

that the ordering is diffusion-controlled particle growth with a zero nucleation rate. In the ordering of BZT, the nucleation due to the formation of regions of critical size with the required B-site order of Zn and Ta is postulated to occur during the pretreatment calcination stage and ramp-to-anneal stages. Similarly, in α-CuAl, the short-range order developed during the low-temperature and pretreatment stages is proposed to act as the nucleation site for the development of long-range order. The ordering in Ni_3Al also proceeds by similar mechanisms as for BZT with the exponent $n = 1.1$.[26]

The rate of ordering, *k*, shows an approximately 10-fold increase between 1300 and 1500 °C. The OP_0 values are essentially the same at all temperatures except at 1450 °C, where the higher degree of "initial" order can be attributed to the time spent at 1200 °C prior to stepping up the temperature to 1450 °C. The OP_∞ shows an increase in the final level of ordering as the temperature of annealing is increased. This is somewhat contrary to expectation if it is assumed that thermodynamic equilibrium is limiting the degree of ordering. Accordingly, it must be assumed that kinetic considerations determine the final ordering, which also suggests that at 1500 °C, BZT is still well below its order−disorder transition temperature, reported to be approximately 1600 °C.[27]

During the data analysis, it was apparent that the position of the calculated (001) peak did not match the observed position of the reflection (see Figure 6). Refinement of the unit-cell dimensions is heavily weighted toward the strong subcell reflections, which are typically some 3 orders of magnitude more intense than the supercell reflections. Because a common set of cell dimensions is used for both histograms of data at each temperature, the conclusion is that there is a subtle difference in the cell parameters between the ordered and disordered phases. The misfit of the (001) peak is most marked at 1300 °C, becoming less significant as the temperature increases.

The refinements were improved by introducing a second set of unit-cell parameters to model the supercell reflection positions in the second histogram. Sequential refinements were then rerun for each experiment to give a much improved fit in terms of the refined position for the (001) peak and a better modeling of the peak shape. An example of the improved fit is shown in Figure 6. This refinement strategy allowed the extraction of independent sets of lattice parameters corresponding to the supercell reflections and the subcell reflections from each histogram in the refinements. Figure 7 shows the comparison between the sub- and supercell lattice parameters for the 1300 °C experiment. There is a wide scatter of the cell parameter values for the supercell reflections at the beginning of the experiments when the reflections are very weak; however, beyond this region, the difference between sub- and supercell lattice parameters

(26) Cardellini, F.; Contini, V.; Mazzone, G. *Scr. Metall. Mater.* **1995**, *32*, 641−646.
(27) Reaney, I. M.; Colla, E. L.; Setter, N. *Jpn. J. Appl. Phys., Part 1* **1994**, *33*, 3984−3990.

Table 2. Mean Difference in Sub- and Supercell Lattice Parameters Determined over the Final 2000 s of the Annealing Period

T (°C)	$a_{supercell} - a_{subcell}$ (Å)	$c_{supercell} - c_{subcell}$ (Å)	$V_{supercell} - V_{subcell}$ (Å^3)
1300	−0.0047(7)	0.037(3)	0.78(15)
1400	−0.0038(7)	0.031(4)	0.64(12)
1450	0.0052(8)	0.09(3)	0.63(11)
1500	−0.006(7)	0.004(4)	0.10(14)

is essentially constant over the time period of the experiments, even once ordering had reached the maximum value, allowing mean values for the discrepancy to be calculated (see Table 2).

At 1300 and 1400 °C, the mean difference in the *a* lattice parameters shows the subcell to be larger than the supercell, although not to a significant degree. The differences in the *c* lattice parameters at these temperatures, however, show a significantly larger value for the supercell. The unit-cell volumes are all larger for the supercell, although the discrepancy diminishes with increasing annealing temperature. At 1500 °C, the *a* and *c* parameters and the cell volume of the sub- and supercells are equivalent within one standard deviation.

A difference in the cell parameters for the sub- and supercell reflections has also been noted in the 1:1 ordered double perovskites Sr_2AlTaO_6 and Sr_2AlNbO_6,[28] although in this case, the cell parameters based on the supercell reflections are smaller than those from the subcell. The ordering process in the BZT system has previously been shown to be complex when examined with high-resolution powder diffraction data ex situ and in situ at 1200 C; ordering is accompanied by separation into two distinct BZT phases due to differences in cation order and Zn content.[10] The cation-ordered form of BZT has a larger unit cell than the disordered form, as discussed below; however, Zn vacancies act to reduce the cell volume, which has been shown in previous ex situ studies[10] to have a more pronounced effect in reducing cell volume compared with the effects of cation ordering. Here, the difference in cell parameters between sub- and supercell observed can be discussed only in terms of the single-phase description of the process permitted by the resolution of the present data and can be explained in part by considering the electrostatic repulsion between cations in adjacent layers in the ordered and disordered material. Layers within the 1:1 ordered material comprise exclusively $M^{5+}-M^{2+}$ pairs, whereas layers within the disordered material will have some $M^{5+}-M^{5+}$ pairs. The 1:1 ordering produces more favorable cation pairs, allowing the volume reduction. The 2:1 ordering of BZT, however, can result in more unfavorable pairs compared to a disordered phase. For example:

- Ordered Ta−Ta−Zn−Ta−Ta−Zn−Ta−Ta−Zn (three Ta− Ta pairs)
- Disordered Ta−Zn−Ta−Zn−Ta−Ta−Ta−Zn−Ta (two Ta− Ta pairs)

Electrostatically unfavorable $M^{5+}-M^{5+}$ pairs can also occur at antiphase boundaries between ordered domains, again tending to an increased repulsion and enlargement of the unit cell. As shown below, the domain size is smaller at higher temperatures and this higher concentration of antiphase domain boundaries would be expected to further enhance the differential in volume between supercell and subcell material. However, as the annealing temperature is increased, the difference between the super- and subcell lattice constants is reduced and becomes insignificant at 1500 °C. The effects of Zn loss are also enhanced at higher temperature and so would appear to be the dominant factor in the present case. There are, however, important distinctions to be made between the present and previous studies. In the earlier study,[10] the high spatial resolution of the diffraction data allowed refinement of two discrete phases in which Zn vacancies were largely confined to the less well ordered phase. In the present lower-resolution study, the characteristics of the phase assemblage cannot be discriminated to this level of detail; however, the larger domains, forming at lower temperatures, do allow better contrast between the more ordered structure corresponding to the supercell reflections compared with the more disordered structure of the domain walls corresponding to the subcell reflections as observed in the lattice parameter differences. This limited degree of discrimination between the ordered and disordered structures is lost at higher temperatures where there is a much higher concentration of domain boundaries.

Domain Growth. Refinement of the data yielded Lorentzian peak width values for both subcell and supercell reflections from the respective histograms. In all experiments, the subcell reflections show an initial rapid sharpening on reaching the annealing temperature corresponding to rapid growth of domains compared with the calcined starting material, followed by a much slower broadening of the peaks as shown in Figure 8. This broadening is explained not in terms of changes to the domain size of the material but as being due to the evolving biphasic nature of BZT:[10,11] the peaks are splitting corresponding to the development of multiple phases; however, the instrumental resolution is insufficient to resolve them fully. In contrast, the supercell peaks exhibit the more expected behavior and sharpen, because of domain growth, to a limiting value as the experiment proceeds (see Figure 8). The supercell peaks are substantially broader than those from the subcell and therefore masks any effects of peak splitting effects due to the biphasic nature of the sample at the latter stages of the annealing process.

The evolution of the domain size, as calculated from the peak widths using eq 1, is shown in Figure 9. The curves were fitted using a KJMA model in an analogous manner to that used for order parameter (*OP*) described above. Values for the rate of domain growth and the extrapolated initial and final domain size are given in Table 3. It should be noted that these values of extrapolated initial domain size p_0 are generally well below the values for the onset of observable superstructure reflections. Given the data quality of the

(28) Woodward, P.; Hoffmann, R. D.; Sleight, A. W. *J. Mater. Res.* **1994**, *9*, 2118−2127.

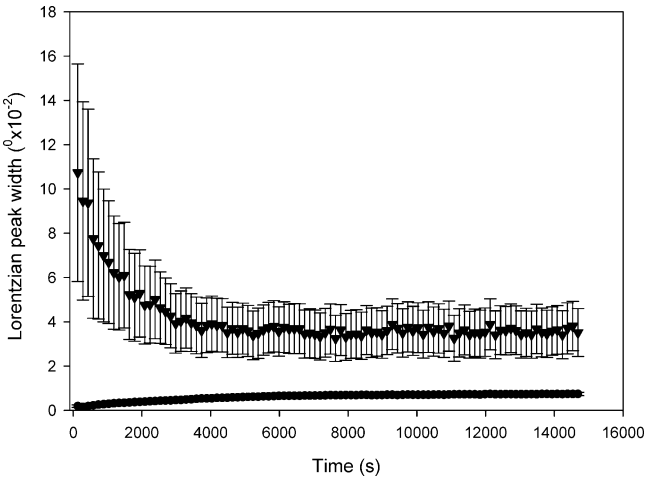

Figure 8. Peak width variation of the BZT super (triangles) and subcell (circles) reflections as a function of annealing time at 1300 °C (for reasons of clarity, only every 10th data point is shown).

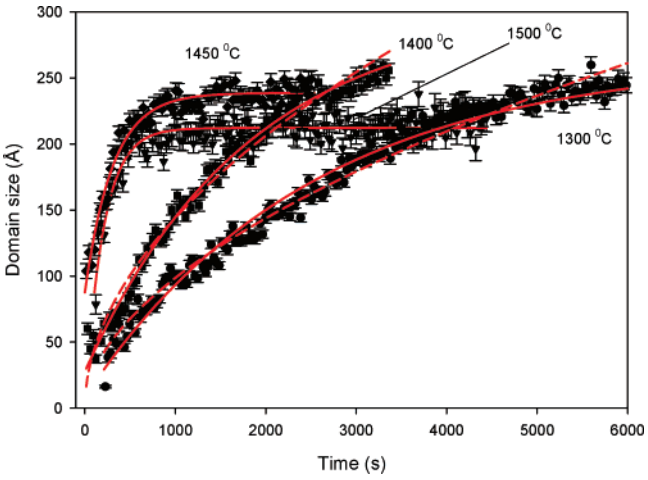

Figure 9. Domain size variation of ordered BZT calculated from peak width values determined from full profile fitting of the super-structure reflections. Solid lines are fits using the modified Avrami function and dotted lines are the fits (to the data at 1300 and 1400 °C only; as explained in the text, this model does not fit at higher temperatures) assuming a Lifshitz−Allen−Cahn model (for reasons of clarity, only every second data point is shown).

current set of experiments and assuming a typical early stage cation order parameter of 0.2, domain sizes of some 60−80 Å are required to produce a (100) superstructure peak observable above background levels. With the exception of the experiment at 1450 °C, which is preceded by the 1200 °C anneal, the derived initial sizes are similar in dimension to the size of the unit cell of the ordered trigonal phase ($c = 7.4$ Å), which is qualitatively consistent with the idea of pre-existing nucleation sites formed in the calcination step at locations where the short-range order fluctuates to above the mean value.

For comparative purposes, peak-width values were also obtained for the (100) peak fitted individually to a simple Lorentzian function at each temperature. The results using this method were found to be broadly consistent with results from the full-profile fits.

Comparing the evolution of the domain size over the different temperature regimes (Figure 9) shows a number of significant features. The general trend is that the rate of domain growth increases with higher annealing temperature. However, the rate at 1450 °C is significantly greater than that at 1400 °C and almost comparable to the results at 1500 °C. A very similar behavior is observed in the rate of cation ordering discussed above. Disregarding the issue of temperature control, the initial anneal of approximately 17 000 s at 1200 °C before the temperature was stepped up to 1450 °C seems a more likely explanation of the apparent discrepancy between the rates. Previous measurements suggest that nuclei of the ordered trigonal phase are formed within the pseudocubic precursor during the calcination and the ramp-to-anneal-temperature stages, with no significant formation of nuclei during annealing.[11] However, if full "site saturation" is not reached prior to annealing, some limited formation of nuclei would be possible. This effect can only be small, otherwise it would not be consistent with the Avrami exponent, n, of 1.0, but an increase in the number of ordered nuclei during the 1200 °C stage would provide more sites for domain growth in the case of the 1450 °C, resulting in the faster than expected rate.

The final observed domain size was ∼225 Å in the 1300 °C experiment, which increases to ∼250 Å, the maximum domain size observed, in the 1400 °C experiment, even though the saturation point was not reached during the experiment. The final domain size then decreased as the annealing temperature is increased in the 1450 and 1500 °C studies. Earlier work following the annealing process at 1200 °C showed the domain size to reach significantly larger values (∼400 Å) than those found in the higher-temperature annealing studies here and to still be increasing after approximately 90 000 s.[11] In this slower kinetic regime, ordering was found to precede domain growth, which was subsequently modeled using the $p \sim t^{1/2}$ relationship according to the Lifshitz−Allen−Cahn (LAC) model, where domain growth is driven by the minimization of curvature of the boundaries.[29] In the present studies, domain growth at 1300 °C and above occurs simultaneously with ordering within the domains. Nevertheless, fitting the data using the $p \sim t^a$ relationship in the current studies proved successful for the 1300 °C (up to a period of 6000 s) and 1400 °C data, with exponents in good agreement with the LAC model found at 1200 °C. The data at 1450 and 1500 °C could not be fitted to this relationship with any reliability because of the clear qualitative difference in the time dependence at these higher temperatures; instead of increasing over the entire measuring time as found at 1300 and 1400 °C, the domain size at the higher temperatures rapidly increases to its final value and then saturates. The refined values of the exponent a are given in Table 4.

At 1200 °C, the loss of Zn is very slow, no evidence for the formation of $Ba_8ZnTa_6O_{24}$ is observed, and the domain growth is unaffected by the formation of impurities. As the annealing temperature is increased, the rate of loss of Zn increases and the formation of $Ba_8ZnTa_6O_{24}$ is observed in the later stages of the 1300 °C (after 5250s) and 1400 °C (after 3000 s) experiments. At these temperatures, the domain size growth initially follows the LAC relationship but, as

(29) Allen, S. M.; Cahn, J. W. *Acta Metall.* **1979**, *27*, 1085−1095.

Table 3. Fitted Parameters for the Domain Growth at Each Temperature According to the Modified KJMA Model: $p(t) = p_0 + (p_\infty - p_0)(1 - \exp(-kt)^n)$

	1300 °C	1400 °C	1450 °C	1500 °C
k (s^{-1})	$3.87(5) \times 10^{-4}$	$6.03(2) \times 10^{-4}$	$3.25(1) \times 10^{-3}$	$4.89(3) \times 10^{-3}$
initial domain size (Å)	10.6(16)	25.9(16)	87.6(27)	4.1(12)
final domain size (Å)	267.7(8)	301.8(3)	238.5(7)	211.9(6)

Table 4. Fitted Parameters to the Lifshitz−Allen−Cahn Model for Domain Growth ($p \propto t^a$)

	1300 °C	1400 °C	1450 °C	1500 °C
a	0.462(6)	0.508(7)	0.153(6)	0.092(5)

the concentration of impurity builds up, the growth rate deviates from the model, in line with the point of initial observation of the formation of $Ba_8ZnTa_6O_{24}$. At 1450 and 1500 °C, the rapid rate of Zn loss and concomitant formation of significant amounts of $Ba_8ZnTa_6O_{24}$ is too rapid and at no point does domain growth follow the $p \propto t^{1/2}$ relationship and the domain growth rapidly stagnates. This increased concentration of impurity phase at higher temperatures also appears to restrict the maximum domain size attained at these temperatures. However, in the case of the 1450 °C experiment the increased nucleation during the 1200 °C annealing period and the larger initial domain size (Table 3) may also result in more domains forming initially and so impinging sooner and restricting the growth. The observed nonmonotonic variation of domain size with temperature therefore correlates well with the change in form of the time dependence of domain-size growth. This suggests that the introduction of Zn vacancies, at high annealing temperatures or after prolonged annealing times at lower temperatures, is an important factor in controlling the rate of diffusion of the B-site cations. The perovskite phase itself is able to accommodate B-site Zn vacancies[10] and these may be important in the local mechanism of cation transport involved the B-site ordering. The $Ba_8ZnTa_6O_{24}$ phase appears when the Zn vacancy content increases beyond the level that can be accommodated in the cubic perovskite structure and the existence of zinc vacancies in both trigonal and cubic components of the phase assemblage may change the mechanism of Zn transport.

The effect of restricted domain growth has been extensively investigated with respect to aluminum nitride precipitates in steel. The AlN precipitates are found to interfere with the normal nucleation and growth of the grains.[30,31] It has been shown that above about 1000 °C, the limit imposed on grain growth by AlN precipitates is removed as they melt.[32] Domain growth occurs by the movement of domain boundaries and this movement is affected by the presence of a second phase, the $Ba_8ZnTa_6O_{24}$ phase in the case here of BZT. The moving boundaries are found to attach to the particles of the second phase, which exert a pinning force and restrict the motion of the boundary.[33,34] This slows and eventually curtails domain growth and restricts the maximum grain size.

Conclusion

The in situ investigation of the high-temperature annealing of BZT using high-count-rate X-ray powder diffraction has given insight into the rates and mechanisms of ordering and domain growth that occur during commercial processing of these microwave resonators. The range of temperatures investigated in the current study allows the calculation of the activation energy for cation transport in BZT using two postulated models describing the cation ordering. Considering that the ordering process requires the positional exchange of neighboring Zn and Ta cations on octahedral sites, the resulting values for the activation energies are physically sensible, being consistent with previous observations of cation transport in oxides where single cations are moving over the available sites within the solid and suggesting similarities between the exchange of both identical (simple diffusion) and dissimilar (cation ordering) cations. Zinc vacancies on the B-site[10] may be important in the processes involved in mobility. The $n = 1$ exponent is observed at the lower temperature initially studied as well as the higher temperatures here and is consistent with no significant increase in the number of nuclei during the measurement period ("site saturation"), consistent with nuclei corresponding to short-range-ordered regions forming in the calcination and ramp-to-anneal stages and growth at a two-dimensional interface. The results highlight the problems associated with the optimization of the Q parameter for commercial resonators. Q is promoted with increased cation ordering, and thus higher ~1500 °C temperatures are seemingly optimal. However, increased Zn loss at these higher temperatures is found to restrict domain growth and the concomitant increase in the concentration of domain walls has been shown to be detrimental to the value of Q.[35] The Zn-deficient 816 phase is implicated in controlling the extent to which domain growth is possible at temperatures sufficiently high to volatilize zinc.

The high count rates for the experiments allowed the collection of data at a uniquely high-time resolution for this type of investigation, while providing refineable powder diffraction data and yielding quantitative structural information even for the most rapid processes. In addition, the technical difficulty of recording powder diffraction data of this quality under well-controlled temperatures up to

(30) Leslie, W. C.; Rickett, R. L.; Dotson, C. L.; Walton, C. S. *Trans. Soc. Met.* **1954**, *46*, 1470−1499.
(31) Rickett, R. L.; Kalin, S. H.; Mackenzie, J. T. *Trans. Inst. Min. Mettal.* **1949**, *185*, 242−251.
(32) Hall, D.; Bennett, G. H. J. *J. Iron Steel Inst.* **1967**, *205*, 309-&.
(33) Leap, M. J.; Brown, E. L. *Mater. Sci. Technol.* **2002**, *18*, 945−958.
(34) Porter, D. A.; Easterling, K. E. *Phase Transformations in Metals and Alloys*; Chapman and Hall: London, 1981.
(35) Davies, P. K.; Tong, J. Z.; Negas, T. *J. Am. Ceram. Soc.* **1997**, *80*, 1727−1740.

1500 °C should not be underestimated. The present methodology is likely to be particularly useful in understanding and refining the optimal processing conditions of the related cobalt−niobate ($Ba_3(Zn/Co)Nb_2O_9$) resonator systems, which are prepared using a more complex annealing sequence at temperatures both above and below the order−disorder temperature. The present study has lower angular resolution than the initial lower temperature study and thus cannot directly address phase-separation of fully and partially ordered BZT phases required for a complete description of the ordering process. However, the ability to measure the ordering kinetics at a range of temperatures affords the activation energies controlling both cation site order and domain growth.

Acknowledgment. We thank EPSRC for Portfolio Partnership support (EPSRC/C511794), the STFC Centre for Materials Physics and Chemistry for partial support (CMPC03106) of P.M.M. and the ESRF for provision of synchrotron beamtime.

Supporting Information Available: Table of fractional coordinates for trigonal BZT using the anti-site model; table of fractional coordinates for trigonal BZT using the stacking-fault model; figures showing variation of the *a* and *c* lattice constants and unit-cell volume at 1300, 1400, 1450, and 1500 °C determined from subcell (triangles) and supercell (circles) reflections.

CM071249J